# Effect of Yielding on the Viscoelastic Response of Amorphous Glassy Polymers

**ALEKSEY D. DROZDOV**

Institute for Industrial Mathematics, 4 Hanachtom Street, Beersheba, 84311 Israel

*Received 19 August 1999; accepted 28 March 2000*

**ABSTRACT:** Constitutive equations are derived for the nonlinear viscoelastic behavior of amorphous glassy polymers. The model is based on the theory of cooperative relaxation in a version of the trapping concept. Stress–strain relations are applied to fit experimental data for polycarbonate in the sub-yield and post-yield regions. Fair agreement is demonstrated between observations and results of numerical simulation. It is revealed that yielding causes substantial changes in the energy landscape of amorphous polymers. © 2001 John Wiley & Sons, Inc. J Appl Polym Sci 80: 2383–2393, 2001

**Key words:** amorphous polymers; viscoelasticity; viscoplasticity; trapping concept; energy landscape

## INTRODUCTION

This paper is concerned with the viscoelastic and viscoplastic behavior of amorphous glassy polymers at the first stage of inelastic deformation when no plastic alignment of long chains occurs and the material remains isotropic at the macrolevel.[1,2] Constitutive equations in viscoplasticity of amorphous polymers are traditionally postulated by analogy with those for crystalline materials[3–6] Three shortcomings of this approach may be mentioned:

1. Viscoplasticity of amorphous and crystalline media are driven by different physical mechanisms.[7] Yielding of crystalline materials is conventionally associated with propagation of glide dislocations, which are not observed in polymers.[8] On the other hand, the substantial effect of pressure on the yield strain[9,10] is typical of amorphous polymers and is not revealed in most metals.
2. Two types of yielding, ductile (caused by shear banding) and brittle (induced by crazing), are not distinguished.[11]
3. The yield point and the residual stresses (strains) are severely affected by the material viscosity which makes problematic the very definition of plasticity in experiments[12] and stimulates attempts to describe the mechanical response of amorphous polymers in the framework of nonlinear viscoelasticity.[13,14]

Interaction between plastic flow and stress relaxation in amorphous and semicrystalline polymers has attracted substantial attention in the past decade. Unlike early studies concerned mainly with the influence of viscosity on the yield stress,[12,15,16] recent works concentrate on the analysis of plasticity-induced changes in relaxation spectra.[17–19]

The viscoplastic behavior of polymers at relatively small strains is conventionally treated as a result of chain-segment rotation.[20–22] A disadvantage of this approach is that it requires unrealistic activation volumes[16] and activation energies[23] to fit observations. Physically plausible val-

*Correspondence to:* A.D. Drozdov (aleksey@cs.bgu.ac.il).

Journal of Applied Polymer Science, Vol. 80, 2383–2393 (2001)

ues of adjustable parameters may be found, provided rotation of individual strands is replaced by cooperative rearrangement of long chain when scores of neighboring strands simultaneously change their position.[16] The pattern of "regions of large shear stresses" was introduced in the early 1980s[24,25] to describe the response of metallic glasses based on the concept of "islands of mobility",[26] and it is conceptually close to the Adam–Gibbs theory[27] for the viscoelastic behavior of amorphous polymers. An important question in modeling the time-dependent response of amorphous media is whether the cooperative regions responsible for viscoelastic and viscoplastic phenomena have the same length scale.

The correlation length for viscoelastic flow units[28] has been thoroughly studied in the recent years, and it is estimated as 0.5–1.5 nm in the vicinity of the glass transition temperature $T_g$.[29,30] Direct measurements of the characteristic size of plastic $\tau$-defects[23] are absent, whereas calculations based on the activation volume model provide values in the range of 10 nm.[7] This size may be treated as a lower limit, whereas other sources give essentially higher values of the order of $10^3$ nm.[8,11,31,32]

With reference to these data, we assume that the characteristic length of plastic regions substantially exceeds that for viscoelastic flow units. Because any plastic island of mobility contains a large number of viscoelastic regions, only properties of an "average" rearranging domain may be taken into account. This assumption implies that at the first stage of yielding, when the specimen remains homogeneous at the macro-level, changes in the viscoelastic response are determined by the current level of strains only, both for ductile and brittle modes of fracture.

The objective of this study is to derive a constitutive model that accounts for the effect of yielding on relaxation spectra of amorphous polymers and to verify stress–strain relations by comparison of experimental data for polycarbonate with results of numerical simulation.

Adopting the trapping concept,[33–35] we treat a glassy polymer as an ensemble of cages where flow units are trapped. In the phase space, any cage is thought of as a potential well on the energy landscape, at the bottom level of which a flow unit is located. Because of thermal fluctuations, flow units can hop to higher energy levels, but they cannot leave their traps (the pattern of ergodicity breaking[36]).

Referring to the transition-state theory,[37] we suppose that some liquid-like (reference) state exists on the energy landscape, where flow units change their configurations. When a region reaches the liquid-like level in a hop, stresses totally relax in it. If a flow unit hops below the reference level, it lands in its potential well without changes. The depth of a potential well with respect to the reference state of a stress-free material is determined by its energy $w$. We set $\omega = 0$ for the initial reference state and $w > 0$ for an arbitrary trap. With reference to the random energy model,[39] the distribution of traps with various potential energies $w$ is described by the Gaussian formula

$$p(w) = \frac{1}{\sqrt{2\pi}\,\Sigma} \exp\left[-\frac{(w - W)^2}{2\,\Sigma^2}\right] \qquad (1)$$

with the mean value $W$ (which characterizes the average energy of a disordered medium) and the standard deviation $\Sigma$. Equation 1 is applicable provided that the probability of traps with negative energies is small compared to unity

$$\int_{-\infty}^{0} p(w)\,dw \ll 1 \qquad (2)$$

The viscoelastic response of glassy polymers is modeled as a sequence of random hops of rearranging regions (driven by thermal fluctuations) with respect to a fixed energy landscape.[38] For a linear material, the liquid-like energy level is fixed, and relaxing regions are treated as linear elastic media. To predict the nonlinear behavior, we assume that the reference level changes its position with respect to the free energy hypersurface and the response of individual flow units is nonlinear.

Viscoplasticity of amorphous polymers is modeled as time-varying transformations of the energy landscape. We propose the following scenario for active uniaxial loading (the strain $\epsilon$ monotonically increases) based on the random energy model (eq. 1). The mean energy of a disordered medium $W$ is independent of mechanical factors and temperature $T$ (an analog of the conservation law for the potential energy of cages). Below the yield point, the distribution of traps is independent of strains and $\Sigma$ is constant. At the yield point, the quantity $\Sigma$ suffers a positive jump, which reflects activation of "regions of large shear

stresses" induced either by formation of shear bands or by crazing. In the post-yield region, the standard deviation of potential energies of cages $\Sigma$ monotonically increases with strains, which reflects "propagation of plastic defects".

The study aims to describe in detail changes in the viscoelastic response of amorphous polymers driven by yielding and to support this scenario by experimental data for polycarbonate. The paper is divided into sections dealing with the kinetics of rearrangement of flow units (see Rearrangement of Flow Units), derivations of nonlinear constitutive equations for a polymer (see Stress–Strain Relationships), comparison of stress–strain relations with observations (see Comparison with Experimental Data), and concluding remarks (see Conclusions).

## REARRANGEMENT OF FLOW UNITS

Let $q(\omega)\mathrm{d}\omega$ be the probability for a flow unit to reach (in a hop) the energy level that exceeds the bottom level of its potential well by some value belonging to the interval $[\omega, \omega + \mathrm{d}\omega]$. According to the extreme-value statistics,[40] we set $q(\omega) = \alpha\exp(-\alpha\omega)$, where $\alpha$ is a material constant. The current position of the liquid-like energy level with respect to the reference level of a stress-free medium is denoted as $-\Omega(t)$ [in agreement with observations, we suppose that external loads cause a descent of the liquid-like level]. The probability for a relaxing region in a trap with the current potential energy $w$ to reach the reference state in an arbitrary hop is given by

$$Q(t, w) = \int_{w-\Omega(t)}^{\infty} q(\omega)\, d\omega = \exp[-\alpha(w - \Omega(t))] \tag{3}$$

The average rate of hops in a cage $\Gamma$ is assumed to depend on temperature $T$ only. Confining ourselves to isothermal processes, we treat $\Gamma$ as a constant. Multiplying $\Gamma$ by the probability to reach the reference state in a hop $Q$, we find the rate of rearrangement in a trap with the current potential energy $w$

$$L(t, w) = \Gamma\, \exp[-\alpha(w - \Omega(t))] \tag{4}$$

Denote by $\Xi_0$ the (time-uniform) concentration of traps per unit mass and by $\Xi(t, \tau, w_0)$ the current concentration of traps that had potential energy $w_0$ before loading and where the last rearrangement had occurred before time $\tau < t$. Let $w = w(t, w_0)$ be the current (at time $t$) potential energy of a cage that had the energy $w_0$ before loading. Equating the relative rates of reaching the liquid-like state to $L$, we arrive at the differential equations

$$\frac{\partial \Xi}{\partial t}\,(t, 0, w_0) = -L(t, w(t, w_0))\Xi(t, 0, w_0) \tag{5}$$

$$\frac{\partial^2 \Xi}{\partial t \partial \tau}\,(t, \tau, w_0) = -L(t, w(t, w_0))\,\frac{\partial \Xi}{\partial \tau}\,(t, \tau, w_0) \tag{6}$$

Because flow units cannot leave their cages, the function $\Xi(t, \tau, \omega_0)$ is connected with the initial probability density of traps $p(\omega_0)$ by the formula

$$\Xi(t, t, w_0) = \Xi_0 p(w_0) \tag{7}$$

The concentration of relaxing regions in traps with initial potential energies located in the interval $[\omega_0, \omega + \mathrm{d}\omega_0]$ that rearrange per unit time equals $\Xi_0 L(t, \omega(t, \omega_0))p(\omega_0)\mathrm{d}\omega_0$. Neglecting the duration of a hop (a few picoseconds[35]) compared with the characteristic time of stress relaxation, we find that the same number of flow units land in their traps per unit time

$$\frac{\partial \Xi}{\partial \tau}\,(t, \tau, w_0)\big|_{t=\tau} = \Xi_0 L(\tau, w(\tau, w_0))p(w_0) \tag{8}$$

The solutions of eqs. 5 and 6 with initial conditions in eqs. 7 and 8 read

$$\Xi(t, 0, w_0) = \Xi_0 p(w_0)\exp\left[-\int_0^t L(s, w(s, w_0))\, ds\right] \tag{9}$$

$$\frac{\partial \Xi}{\partial \tau}\,(t, \tau, w_0) = \Xi_0 p(w_0) L(\tau, w(\tau, w_0)) \times \exp\left[-\int_\tau^t L(s, w(s, w_0))\, ds\right] \tag{10}$$

## STRESS–STRAIN RELATIONS

Because a flow unit totally relaxes when it reaches the liquid-like state, its natural (stress-

free) configuration coincides with the actual (deformed) configuration of the bulk medium at the instant of rearrangement. For uniaxial deformation, the strain from the natural configuration of a relaxing region to its actual configuration at time $t$ is given by

$$\epsilon_*(t, \tau) = \epsilon(t) - \epsilon(\tau) \tag{11}$$

where $\epsilon$ is the macro-strain, and $\tau \le t$ is the last instant when the region has rearranged. The mechanical energy of a flow unit $U(\epsilon_*(t, \tau))$ satisfies the conditions

$$U(0) = 0 \quad \text{and} \quad \frac{\partial U}{\partial \epsilon}(0) = 0 \tag{12}$$

Summing the mechanical energies of flow units and neglecting the energy of their interaction, we find the mechanical energy of an amorphous polymer (per unit mass)

$$\Phi(t) = U(\epsilon(t)) \int_0^\infty \Xi(t, 0, w_0)\, dw_0 + \int_0^t U(\epsilon(t) - \epsilon(\tau))\, d\tau \int_0^\infty \frac{\partial \Xi}{\partial \tau}(t, \tau, w_0)\, dw_0 \tag{13}$$

At small strains, the stress $\sigma$ is expressed in terms of the strain $\epsilon$ by the formula

$$\sigma(t) = \rho \frac{\partial \Phi(t)}{\partial \epsilon(t)} \tag{14}$$

where $\rho$ is mass density in the stress-free state. Substitution of eq. 13 into this equality results in the constitutive equation

$$\sigma(t) = \rho \left[ \frac{\partial U}{\partial \epsilon}(\epsilon(t)) \int_0^\infty \Xi(t, 0, w_0)\, dw_0 + \int_0^t \frac{\partial U}{\partial \epsilon}(\epsilon(t) - \epsilon(\tau))\, d\tau \int_0^\infty \frac{\partial \Xi}{\partial \tau}(t, \tau, w_0)\, dw_0 \right] \tag{15}$$

For conventional relaxation tests with

$$\epsilon(t) = 0 \quad (t < 0) \qquad \text{and} \qquad \epsilon(t) = \epsilon \quad (t > 0) \tag{16}$$

eqs. 10 and 15 imply that

$$E(t, \epsilon) = E_0(\epsilon) \int_0^\infty p(w_0) \times \exp\left[ - \int_0^t L(s, w(s, w_0))\, ds \right] dw_0 \tag{17}$$

where

$$E(t, \epsilon) = \frac{\sigma(t)}{\epsilon} \quad \text{and} \quad E_0(\epsilon) = \rho \Xi_0 \frac{1}{\epsilon} \frac{\partial U}{\partial \epsilon}(\epsilon) \tag{18}$$

We assume that the position of the reference state $\Omega$ is uniquely determined by the current strain $\epsilon$, $\Omega = \Omega_0(\epsilon)$, substitute eqs. 1 and 4 into eq. 17 and arrive at the formula

$$E(t, \epsilon) = \frac{E_0(\epsilon)}{\sqrt{2\pi}\, \Sigma} \int_0^\infty \times \exp\left[ - \left( \frac{(w_0 - W)^2}{2\Sigma^2} + \Theta(\epsilon) \exp(-\alpha w) t \right) \right] dw_0 \tag{19}$$

where

$$\Theta(\epsilon) = \Gamma \exp[\alpha \Omega_0(\epsilon)] \tag{20}$$

For the Gaussian distribution of energies of cages (eq. 1), transformation of the energy landscape may be described by the linear function

$$w = A w_0 + B \tag{21}$$

where the coefficients $A$ and $B$ are determined by mechanical factors. It follows from the energy conservation law $\mathrm{E}w = \mathrm{E}w_0$, where E denotes the mathematical expectation, that $B = (1 - A)W$. This equality together with eq. 21 implies that

$$w_0 - W = \frac{w - W}{A} \tag{22}$$

Combining this formula with eq. 19 and bearing in mind that for relaxation tests, $A$ is a function of strain $\epsilon$, we find that

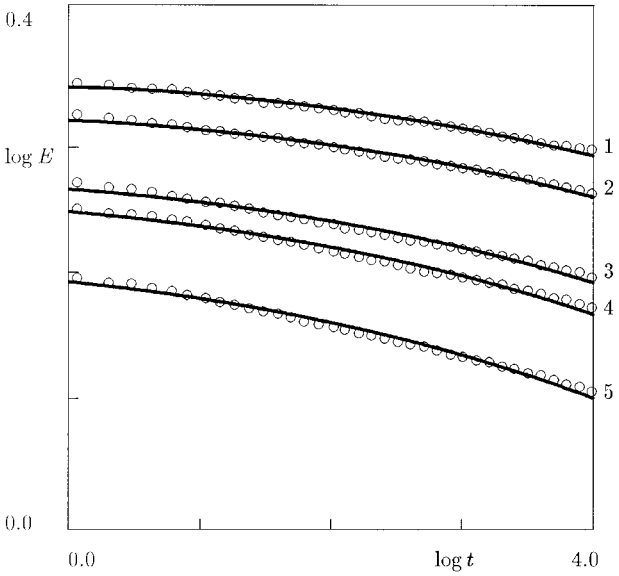


**Figure 1** The Young modulus $E$ (GPa) versus time $t$ (s) for polycarbonate at room temperature. Key: (○) experimental data;[44] (—) predictions of the model with $\Sigma_* = 10.4$; (curve 1) $\epsilon_1 = 0.01$; (curve 2) $\epsilon_1 = 0.015$; (curve 3) $\epsilon_1 = 0.02$; (curve 4) $\epsilon_1 = 0.025$; (curve 5) $\epsilon_1 = 0.03$.

$$E(t, \epsilon) = \frac{E_0(\epsilon)}{\sqrt{2\pi}\,\Sigma_0(\epsilon)} \int_0^\infty \times \exp\left[-\left(\frac{(w - W)^2}{2\,\Sigma_0^2(\epsilon)} + \Theta(\epsilon)\exp(-\alpha w)t\right)\right] dw \quad (23)$$

where $\Sigma_0(\epsilon) = A(\epsilon)\Sigma$. In the new notation $z = \alpha\omega$, $W_* = \alpha W$, and $\Sigma_* = \alpha\Sigma_0$, this equality reads

$$E(t, \epsilon) = \frac{E_0(\epsilon)}{\sqrt{2\pi}\,\Sigma_*(\epsilon)} \int_0^\infty \times \exp\left[-\left(\frac{(z - W_*)^2}{2\,\Sigma_*^2(\epsilon)} + \Theta(\epsilon)\exp(-z)t\right)\right] dz \quad (24)$$

Equation 24 is determined by two adjustable parameters, $\Gamma$ and $W_*$, and three material functions, $E_0(\epsilon)$, $\Sigma_*(\epsilon)$, and $\Omega_*(\epsilon)$, where $\Omega_* = \alpha\Omega_0$. Because one of the constants $\Gamma$ and $W_*$ in eq. 24 may be chosen arbitrarily, we set $W_* = 20$ in fitting observations. At small strains, the functions $E_0$ and $\ln \Theta$, and $\Sigma_*$ are approximated by the following linear dependencies, respectively:

$$E_0(\epsilon) = a_0 - a_1\epsilon \quad (25)$$

$$\ln \Theta(\epsilon) = b_0 + b_1\epsilon \quad (26)$$

$$\Sigma_*(\epsilon) = c_0 + c_1\epsilon \quad (27)$$

with parameters $a_k$, $b_k$, and $c_k$ found by matching observations.

## COMPARISON WITH EXPERIMENTAL DATA

To validate eq. 24, we fit observations in tensile and torsional relaxation tests for polycarbonate. We begin with experimental data measured in the sub-yield region at room temperature. For a detailed description of the experimental procedure, see Colucci et al.[41] Figure 1 demonstrates fair agreement between experimental data and results of numerical simulation with strain-independent parameters $W_*$ and $\Sigma_*$ (yielding is neglected). Figure 2 shows that eqs. 25, 26 adequately predict the effect of strains on the Young modulus $E_0$ and the rate of hops $\Theta$.

To analyze transition from the nonlinear viscoelastic to viscoplastic behavior, we match observations for polycarbonate at various temperatures $T$ from −63 to 67 °C. A description of the experimental procedure can be found in Litt and Torp.[42] Figures 3 and 4 evidence that eq. 24 cor-

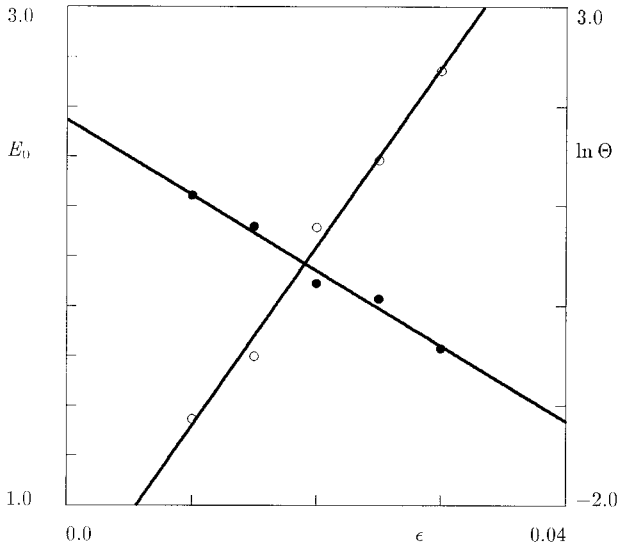


**Figure 2** The parameters $E_0$ (GPa; ●) and $\Theta$ ($s^{-1}$; ○) versus strain $\epsilon$ for polycarbonate at room temperature. Symbols represent treatment of observations.[41] Solid lines represent approximations of experimental data by eqs. 25, 26, with $a_0 = 2.55$, $a_1 = 30.35$ and $b_0 = -3.00$, $b_1 = 179.40$.

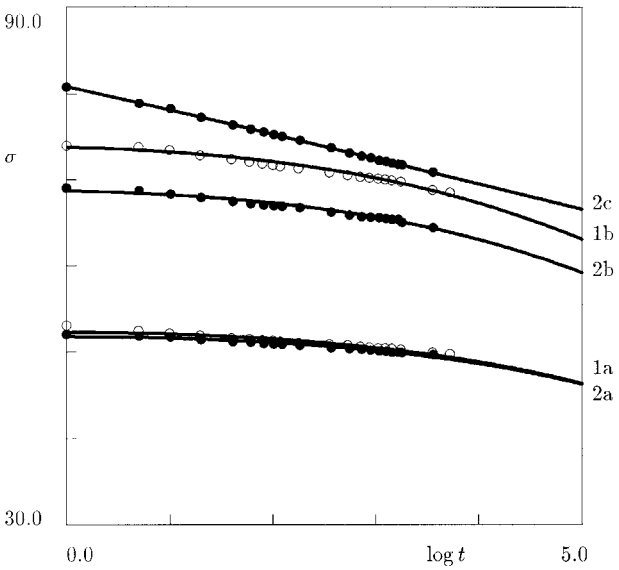


**Figure 3** The stress $\sigma$ (MPa) versus time $t$ (s) for polycarbonate at $T = -63$ °C (○) and $T = -24$ °C (●). Symbols represent experimental data.[42] Solid lines represent their approximation by the model. Curve 1a: $\epsilon = 0.0242$; curve 1b: $\epsilon = 0.0405$; curve 2a: $\epsilon = 0.0254$; curve 2b: $\epsilon = 0.0390$; curve 2c: $\epsilon = 0.0530$.

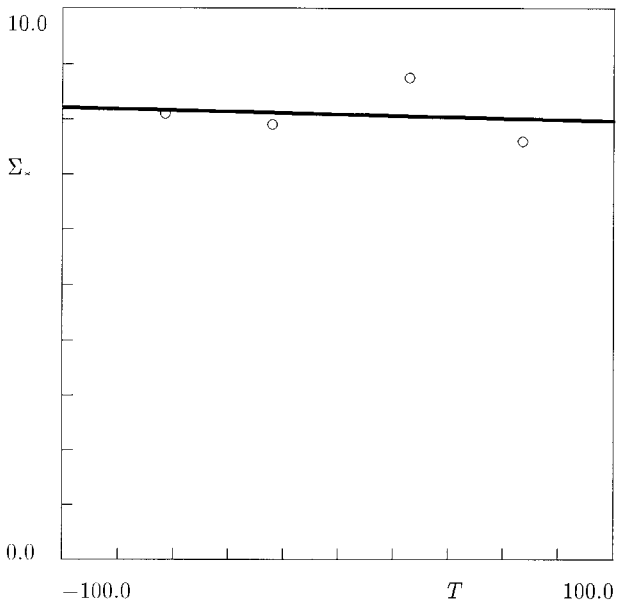


**Figure 5** The parameter $\Sigma_*$ versus temperature $T$ (°C) for polycarbonate in the sub-yield region. Circles represent the treatment of observations.[42] Solid line represents the approximation of experimental data by the linear function $\Sigma_* = \beta_0 + \beta_1 T$, with $\beta_0 = 8.09$ and $\beta_1 = -0.0012$.

rectly predicts relaxation curves in the sub-yield, as well as in the post-yield regions. Figure 5 demonstrates that the standard deviation of energies of traps $\Sigma_*$ is practically independent of temperature in the region of nonlinear viscoelasticity. Figure 6 reveals that this parameter remains constant unless the longitudinal strain $\epsilon$ exceeds the

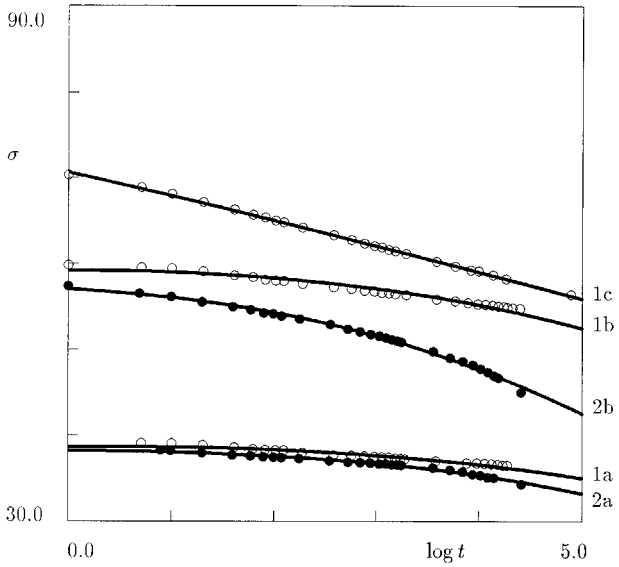


**Figure 4** The stress $\sigma$ (MPa) versus time $t$ (s) for polycarbonate at $T = 26$ °C (○) and 67 °C (●). Symbols represent experimental data.[42] Solid lines represent their approximation by the model. Curve 1a: $\epsilon = 0.185$; curve 1b: $\epsilon = 0.0320$; curve 1c: $\epsilon = 0.0508$; curve 2a: $\epsilon = 0.0193$; curve 2b: $\epsilon = 0.0331$.

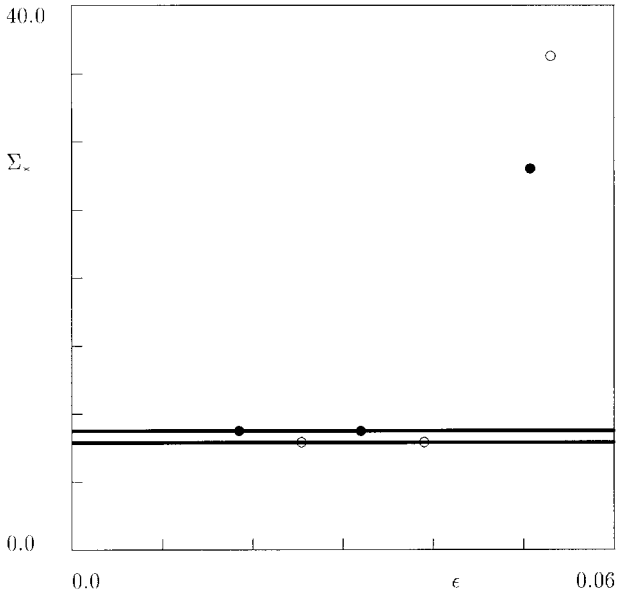


**Figure 6** The parameter $\Sigma_*$ versus strain $\epsilon$ for polycarbonate at $T = -24$ °C (○) and $T = 26$ °C (●). Symbols represent treatment of observations.[42]

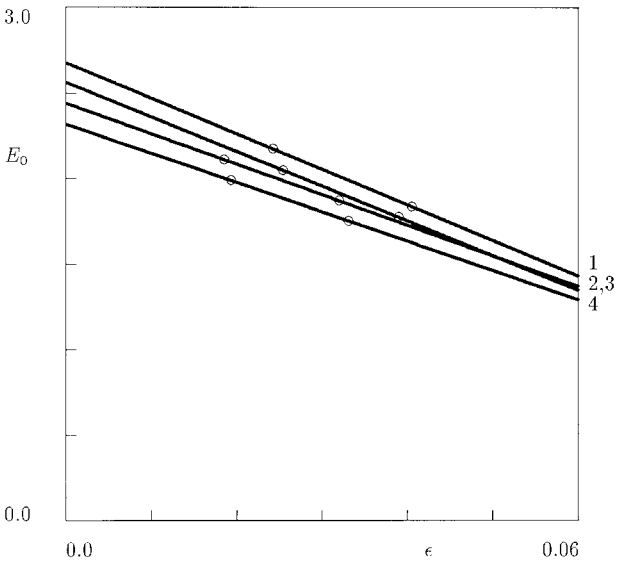


**Figure 7** The initial Young modulus $E$ (GPa) versus strain $\epsilon$ for polycarbonate in the sub-yield region. Circles represent treatment of observations.[42] Solid lines represent approximations of experimental data by eq. 25. Curve 1: $T = -63$ °C, $a_0 = 2.68$, $a_1 = -20.82$; curve 2: $T = -24$ °C, $a_0 = 2.56$, $a_1 = -20.30$; curve 3: $T = 26$ °C, $a_0 = 2.44$, $a_1 = -17.88$; curve 4: $T = 67$ °C, $a_0 = 2.32$, $a_1 = -17.14$.

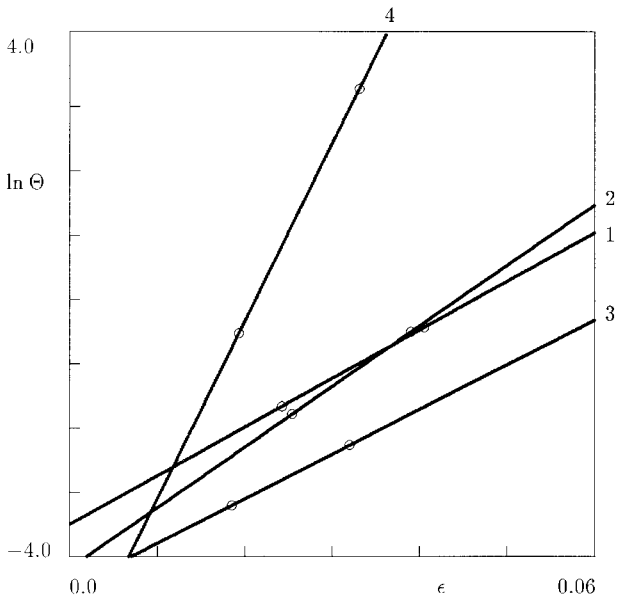


**Figure 8** The parameter $\Theta$ ($s^{-1}$) versus strain $\epsilon$ for polycarbonate in the sub-yield region. Circles represent treatment of observations.[42] Solid lines represent approximations of experimental data by eq. 26. Curve 1: $T = -63$ °C, $b_0 = -3.50$, $b_1 = 73.86$; curve 2: $T = -24$ °C, $b_0 = -4.17$, $b_1 = 92.11$; curve 3: $T = 26$ °C, $b_0 = -4.47$, $b_1 = 67.87$; curve 4: $T = 67$ °C, $b_0 = -5.81$, $b_1 = 270.53$.

yield strain $\epsilon_y$, and it jumps to substantially higher values in the post-yield region. The effect of strain $\epsilon$ on the initial modulus $E_0$ and the rate of hops $\Theta$ is depicted in Figures 7 and 8. Figure 7 demonstrates that eqs. 25–27 correctly predict a decrease in the elastic modulus with strain, and the coefficient $a_1$ is practically independent of temperature $T$. Figure 8 shows that $\Theta$ increases with $\epsilon$, in agreement with eqs. 25–27, and the coefficient $b_1$ weakly depends on temperature $T$ (except for the curve corresponding to $T = 67$ °C). The difference between the coefficient $b_1$ at $T = 67$ °C and that at other temperatures may be explained by changes in the type of yield, when "brittle" yielding driven by crazing turns into "ductile" yielding associated with shear banding.[11]

To study transition from the sub-yield to the post-yield response in detail, we fit experimental data for polycarbonate at $T = 50$ °C. For a detailed description of the experimental procedure, we refer to Ricco and Smith.[43] Fair agreement between results on numerical simulation and experimental data is demonstrated in Figure 9. The parameters $\Sigma_*$, $E_0$, and $\Theta$ are plotted versus the longitudinal strain $\epsilon$ in Figures 10–12.

Figure 10 reveals that the standard deviation of energies of traps $\Sigma_*$ is strain-independent in

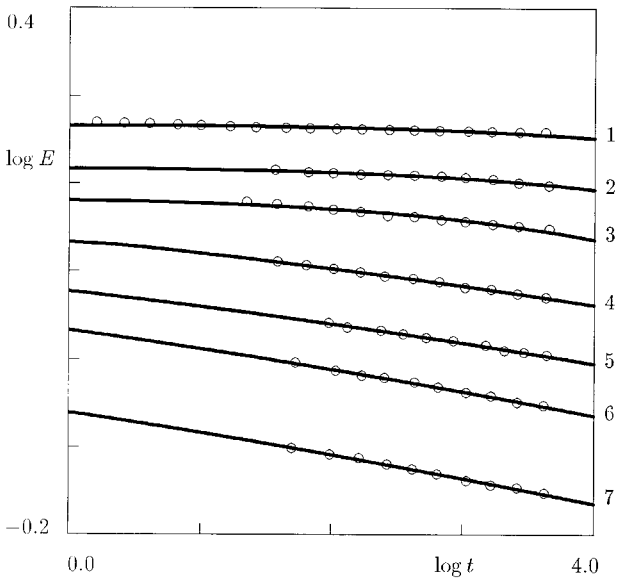


**Figure 9** The Young modulus $E$ (GPa) versus time $t$ (s) for polycarbonate at 50 °C. Circles represent experimental data.[43] Solid lines represent their approximation by the model. Curve 1 $\epsilon_1 = 0.007$; curve 2: $\epsilon_1 = 0.020$; curve 3: $\epsilon_1 = 0.031$; curve 4: $\epsilon_1 = 0.042$; curve 5: $\epsilon_1$ 7 = 0.047; curve 6: $\epsilon_1 = 0.052$; curve 7: $\epsilon_1 = 0.0625$.

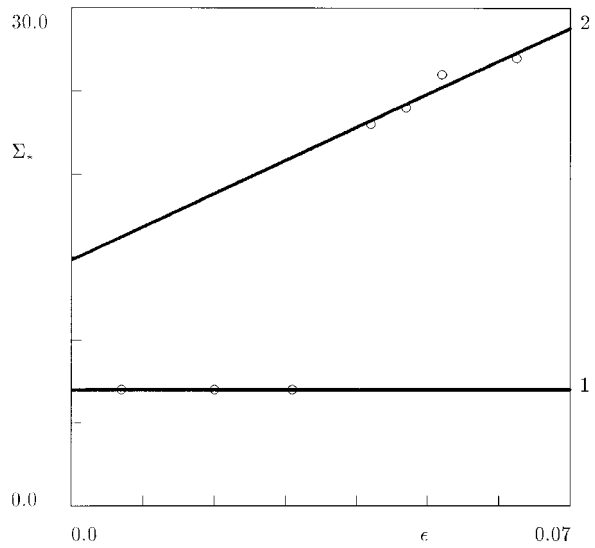


**Figure 10** The parameter $\Sigma_*$ versus strain $\epsilon$ for polycarbonate at 50 °C. Circles represent treatment of observations.[43] Solid lines represent approximation of experimental data by eq. 27, with $c_0 = 7.0$, $c_1 = 0.0$ (curve 1) and $c_0 = 14.83$, $c_1 = 199.84$ (curve 2).

the sub-yield region, and it grows linearly with strain in the post-yield region. According to Figures 1, 5, 6, and 10, practically the same values of $\Sigma_*$ have been found for all three kinds of polycarbonate in the range of temperatures from −70 to 70 °C.

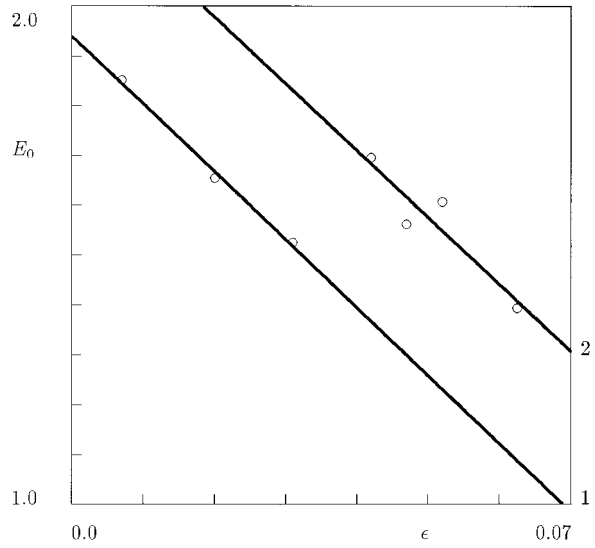


**Figure 11** The initial Young modulus $E_0$ (GPa) versus strain $\epsilon$ for polycarbonate at 50 °C. Circles represent treatment of observations.[43] Solid lines represent approximation of experimental data by eq. 27, with $a_1 = 1.94$, $a_1 = 13.64$ (curve 1) and $a_0 = 2.25$, $a_1 = 13.44$ (curve 2).

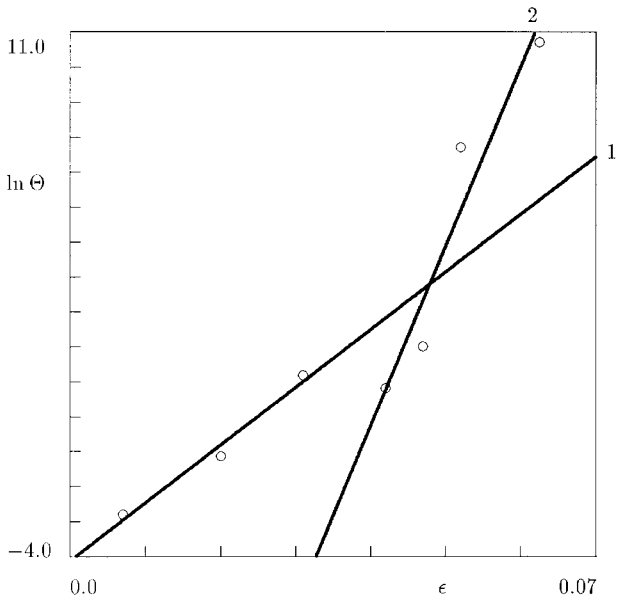


**Figure 12** The parameter $\Theta$ ($s^{-1}$) versus strain $\epsilon$ for polycarbonate at 50 °C. Circles represent treatment of observations.[43] Solid lines represent approximation of experimental data by eq. 26, with $b_0 = -4.12$, $b_1 = 165.21$ (curve 1) and $b_1 = -20.84$, $b_1 = 514.01$ (curve 2).

Figure 11 shows that the initial Young modulus $E_0$ suffers a jump at the yield point, whereas the parameter $a_1$ does not change at transition from the sub-yield region to the post-yield one. To explain the jump of $E_0$ at the point $\epsilon = \epsilon_y$, it suffices to suppose that the rigidity of a relaxing region depends on the potential energy of the cage where it is trapped. This supposition implies that transformation of the energy landscape (eq. 21; which is reflected by an increase in the standard deviation $\Sigma_*$) changes rigidities of flow units and, as a consequence, leads to an increase in the "average" rigidity $E_0$.

Figure 12 demonstrates that the parameter $\Theta$ increases with $\epsilon$, and the rate of its growth in the post-yield region exceeds that in the sub-yield domain. Figures 2 and 12 imply practically the same values of $b_1$ for two kinds of polycarbonate below the yield strain, whereas Figures 8 and 12 result in similar values of $b_1$ in the post-yield region.

According to Figure 5, the parameter $\Sigma_*$ (which determines the energy landscape in the random energy model) weakly depends on temperature far below the glass transition temperature $T_g$.

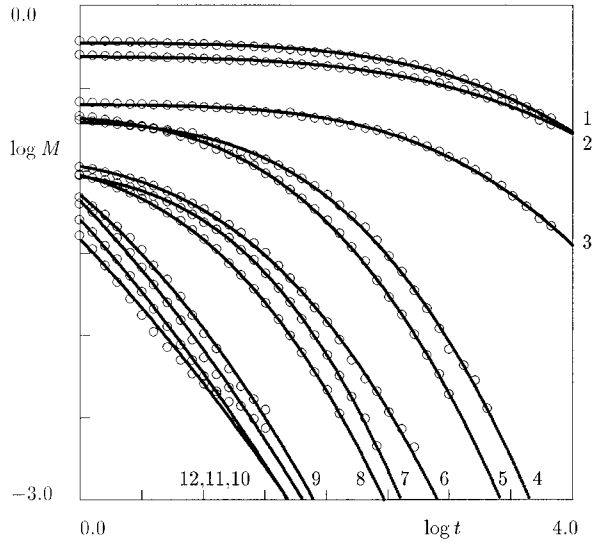


**Figure 13** Torque $M$ (N · m) versus time $t$ (s) for polycarbonate equilibrated at temperature $T$ °C. Circles represent experimental data.[44] Solid lines represent predictions of the model. Curve 1: $T$ = 124.1; curve 2: $T$ = 126.2; curve 3: $T$ =127.3; curve 4: $T$ = 132.5; curve 5: $T$ = 133.2; curve 6: $T$ = 133.9; curve 7: $T$ =135.5; curve 8: $T$ = 135.6; curve 9: $T$ = 138.7; curve 10: $T$ = 139.8; curve 11: $T$ = 139.9; curve 12: $T$ = 140.6.

To analyze the effect of temperature on yielding in the vicinity of $T_g$, we approximate experimental data for equilibrated polycarbonate. For a description of the experimental procedure, see O'Connell and McKenna.[44]

Figure 13 evidences that eq. 24 adequately predicts experimental data in the temperature range from $T_g - 20$ to $T_g$.

According to Figure 14, the standard deviation of energies of traps $\Sigma_*$ decreases with $T$ up to the temperature $T_g = -5$ K, where yielding of the specimen occurs at the strain used in the test, and afterward, $\Sigma_*$ rapidly increases with temperature. The growth of $\Sigma_*$ in the post-yield region qualitatively agrees with results depicted in Figures 6 and 10. In the latter figures, the parameter $\Sigma_*$ increases with strain when the current strain $\epsilon$ exceeds the yield strain $\epsilon_y$ (remaining constant at a fixed temperature), whereas the increase of $\Sigma_*$ observed in Figure14 is driven by a decrease in $\epsilon_y$ with temperature (whereas the current strain $\epsilon$ is constant).

The dependence of the rate of hops $\Theta$ on temperature in the sub-$T_g$ region is plotted in Figure 15. This figure implies that (i) the position of the current liquid-like level $\Omega$ linearly decreases with temperature $T$ both in the sub-yield and in the post-yield regions, but the effect of temperature is stronger when the yield point is crossed; and (ii) fitting data for $\Sigma_*$ and $\Theta$ by the linear functions

$$\ln \Theta = b_0 + b_1 \tag{28}$$

and

$$\Sigma_* = c_0 + c_1 T \tag{29}$$

provides practically the same yield temperature $T_y \approx 137$ °C determined as a temperature at which the coefficients $b_k$ and $c_k$ suffer jumps of amplitude.

## CONCLUSIONS

Constitutive equations have been derived for the nonlinear viscoelastic response of amorphous glassy polymers. The model is based on the theory of cooperative relaxation in a version of the trapping concept. Stress–strain relations are applied to fit experimental data for polycarbonate in tensile and torsional relaxation tests. Fair agreement is demonstrated between results of numer-

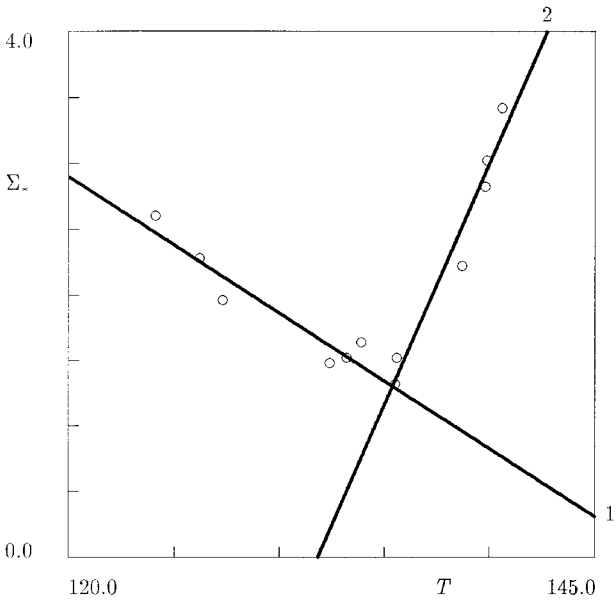


**Figure 14** The parameter $\Sigma_*$ versus temperature $T$ (°C) for equilibrated polycarbonate. Circles represent treatment of observations.[44] Solid lines represent approximation of experimental data by eq. 29, with $c_0$ = 15.32, $c_0$ = −10 (curve 1) and $c_0$ = −48.32, $c_1$ = 0.37 (curve 2).

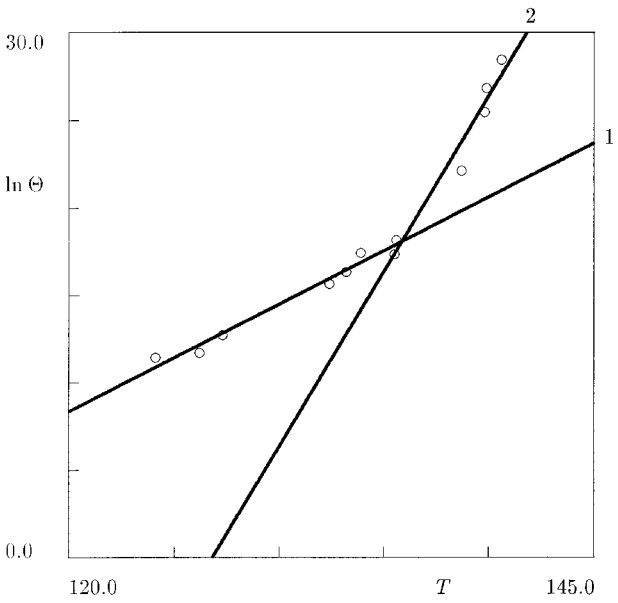


**Figure 15** The parameter $\Theta$ ($s^{-1}$) versus temperature $T$ (°C) for equilibrated polycarbonate. Circles represent treatment of observations.[44] Solid lines represent approximation of experimental data by eq. 28, with $b_0 = 0.61$, $b_1 = 65.35$ (curve 1) and $b_0 = 2.00$, $b_1 = 254.08$ (curve 2).

ical simulation and observations in a wide range of temperatures and strains, which confirms our hypothesis that plastic and viscoelastic cooperative regions have different characteristic lengths. The following conclusions are drawn:

1. The energy landscape of an amorphous polymer is independent of strains in the sub-yield region and it suffers dramatic changes when the yield point is reached. In the post-yield region, an increase in strain causes rather modest changes in the distribution of depths of potential wells.
2. The current energy level of the liquid-like state with respect to the energy landscape $\Omega$ descends with strain $\epsilon$ both in the sub-yield and in the post-yield regions, but the influence of mechanical factors is stronger when the current strain exceeds the yield strain $\epsilon_y$ (Figures 12 and 15).
3. The initial Young modulus $E_0$ monotonically decreases with strain $\epsilon$ except for a yield point, where it may suffer a positive jump (Figure 11) caused by transformation of the energy landscape.

It is worth noting that no qualitative difference has been found between the model parameters for brittle and ductile yielding. This result may be explained by the fact that in both cases the characteristic length of "plastic defects" substantially exceeds that of cooperatively rearranging regions. The difference between the two kinds of yielding may become essential for time-dependent loading processes, which will be the subject of a subsequent study.

Financial support by the Israeli Ministry of Science through grants 9641–1–96 and 1202–1–98 is gratefully acknowledged.

## REFERENCES

1. Boyce, M.C.; Parks, D.M.; Argon, A.S. Mech Mater 1988, 7, 17.
2. Boyce, M.C.; Arruda, E.M. Polym Eng Sci 1990, 30, 1288.
3. Bordonaro. C.M.; Krempl, E. Polym Eng Sci 1992, 32, 1066.
4. Zhang, C.; Moore, I.D. Polym Eng Sci 1997, 37, 414.
5. Krempl, E.; Bordonaro, C.M. Int J Plasticity 1998, 14, 245.
6. Spathis, G.; Kontou, E. Polymer 1998, 39, 135.
7. Mott, P.H.; Argon, A.S.; Suter, U.W. Philos Mag 1993, 67, 931.
8. Kuhlmann-Wilsdorf, D.; Winey, K.I. J Appl Phys 1999, 85, 6392.
9. Pampillo, C.A.; Davis, L.A. J Appl Phys 1971, 42, 4674.
10. Questad, D.L.; Pae, K.D.; Scheinbeim, J.I.; Newman, B.A. J Appl Phys 1981, 52, 5977.
11. Xiao, C.; Jho, J.Y.; Yee, A.F. Macromolecules 1994, 27, 2761.
12. G'Sell, C.; Jonas, J.J. J Mater Sci 1981,16, 1956.
13. Shay, R.M.; Caruthers, J.M. J Rheol 1986, 30, 781.
14. Wineman, A.S.; Waldron, W.K. Polym Eng Sci 1993, 33, 1217.
15. Bauwens-Crowet, C.; Bauwens, J.C.; Homes, G. J Polym Sci, Part A-2 1969, 7, 735.
16. Fotheringham, D.G.; Cherry, B.W. J Mater Sci 1978, 13, 951.
17. Kitagawa, M.; Onoda, T.; Mizutani, K. J Mater Sci 1992, 27, 13.
18. Yoshioka, S.; Usada, H.; Nanzai, Y. J Non-Cryst Solids 1994, 172–174, 765.
19. Ariyama, T. Polym Eng Sci 1994, 34, 1319.
20. Robertson, R.E. J Chem Phys 1966, 44, 3950.
21. Argon, A.S. Philos Mag 1973, 28, 839.
22. Chow, T.S. J Rheol 1992, 36, 1707.
23. Perez, J. Acta Metall Mater 1984, 32, 2163.
24. Srolovitz, D.; Maeda, K.; Vitek, V.; Egami, T. Phil Mag A 1981, 44, 847.
25. Srolovitz, D.; Vitek, V.; Egami, T. Acta Metall Mater 1983, 31, 335.

26. Johari, G.P. J Chem Phys 1973, 58, 1766.
27. Adam, G.; Gibbs, J.H. J Chem Phys 1965, 43, 139.
28. Brawer, S.A. J Chem Phys 1984, 81, 954.
29. Arndt, M.; Stannarius, R.; Groothues, H.; Hempel, E.; Kremer, F. Phys Rev Lett 1997, 79, 2077.
30. Rizos, A.K.; Ngai, K.L. Phys Rev E 1999, 59, 612.
31. Grenet, J.; G'Sell, C. Polymer 1990, 31, 2057.
32. Han, W.; Luo, H.; Teng, F.-E.; Wang, Y.; Panin, V.E.; Slosman, A.I. J Mater Sci Lett 1999, 18, 545.
33. Dyre, J.C. Phys Rev Lett 1987, 58, 792.
34. Bouchaud, J.P. J Phys I France 1992, 2, 1705.
35. Dyre, J.C. Phys Rev B 1995, 51, 12276.
36. Palmers, R.G. Adv Phys 1982, 31, 669.
37. Goldstein, M. J Chem Phys 1969, 51, 3728.
38. Monthus, C.; Bouchaud, J.-P. J Phys A 1996, 29, 3847.
39. Richert, R.; Bäassler, H. J Phys: Condens Matter 1990, 2, 2273.
40. Bouchaud, J.-P.; Mezard, M. J Phys A 1997, 30, 7997.
41. Colucci, D.M.; O'Connell, P.A.; McKenna, G.B. Polym Eng Sci 1997, 37, 1469.
42. Litt, M.H.; Torp, S. J Appl Phys 1973, 44, 4282.
43. Ricco, T.; Smith, T.L. Polymer 1985, 26, 1979.
44. O'Connell, P.A.; McKenna, G.B. J Chem Phys 1999, 110, 11054.